Nigerian Journal of Applied Physics (NJAP)
ISSN Print: 3115-5871
ISSN Online: 3115-588X
DOI: https://doi.org/10.62292/njap-v2i2-2026-40
Volume 2(2), June 2026

# Electron-Phonon Interaction and Electron Energy Loss Function of Spray Pyrolyzed $Cu_2CdSnS_4$ Thin Films at Different Substrate Temperatures

***[1]Michael B. Ochang, [2]Julius N. Tsaviv, [1]Peverga R. Jubu, [1]Zendesha S. Mbalaha, [3]Bunmi J. Akeredolu, [1]Adebayo T. Adepoju, [1]Ngutor S. Akiiga, [1]Augustine A. McAsule, [4,5]Yushamdan Yusof and [6]Kalu Onyekachi**

[1]Department of Industrial Physics, Joseph Sarwuan Tarka University, Makurdi, Nigeria
[2]Department of Chemistry, Joseph Sarwuan Tarka University, Makurdi, Nigeria
[3]Department of Physics, Federal University of Wukari, Wukari, Nigeria.
[4]Nano-Optoelectronic Research and Technology (NOR) Lab, School of Physics, Universiti Sains Malaysia, 11800 USM Penang
[5]School of Physics, Universiti Sains Malaysia, 11800 USM Penang
[6]Department of Physics, Federal University of Lafia, LafiaState, Nigeria.

*Corresponding author's email: bikomchang@yahoo.co.uk

**ABSTRACT**

$Cu_2CdSnS_4$ (CCTS) thin films were successfully synthesized using the spray-pyrolysis method at substrate temperatures of 300 °C, 350 °C, and 400 °C. This study aimed to explore how deposition temperature impacts electron–phonon interaction, surface energy-loss function (SELF), and volume energy-loss function (VELF). X-ray diffraction (XRD) analysis showed a temperature-induced phase transition from the cernyite to the stannite structure, with crystallite size increasing from 32.5 nm to 48.3 nm. A decrease in dislocation density and microstrain, indicating improved crystallinity was noticed. Atomic Force Microscopy (AFM) analysis revealed that surface roughness increased with temperature, suggesting enhanced adatom mobility and grain coarsening. The optical absorption spectra from UV-Vis spectroscopy displayed a red-shift in the absorption edge as the temperature rose, resulting in a band gap reduction from 1.52 eV to 1.31 eV, while the refractive index slightly increased from 2.94 to 3.06. The Urbach energy also rose from 0.372 eV to 0.704 eV, indicating stronger disorder-induced tail states and enhanced electron–phonon coupling. We found that the calculated electron–phonon interaction strength increased as 5.03 eV, 6.83 eV and 8.10 eV with temperature 300 °C, 350 °C, and 400 °C respectively, confirming that carrier–lattice coupling intensifies at higher growth temperatures. Both SELF and VELF increased systematically with temperature, reflecting improved crystallinity, enhanced dielectric resonance, and greater plasmonic activity. These results highlight the significant impact of substrate temperature on lattice dynamics and energy-loss mechanisms in CCTS thin films, which are crucial for optimizing absorber layers in next-generation thin-film solar cells.

**Keywords**: $Cu_2CdSnS_4$, Electron-phonon Interaction, Electron Energy Loss Function.

## INTRODUCTION

Solar cells have become a clean and sustainable alternative to fossil fuels, paving the way to meet the increasing global energy demand and reach our decarbonization targets. They work by converting sunlight directly into electricity through the photovoltaic effect, making them a key player in the future of low-carbon energy systems. However, the efficiency of solar cells is still held back by various intrinsic and extrinsic loss mechanisms, such as charge-carrier recombination, carrier lifetime (Wang et al., 2022; Dizaj, 2025), and charge carrier collection rate (Zhao et al., 2024; Zhu et al., 2020), among others. These factors that limit the high efficiency of solar cells are influenced by electron-phonon interactions (Alkauskas et al., 2014) and energy loss functions like the surface energy loss function (SELF) (Boriskina et al., 2017) and volume energy loss function (VELF) (Nguyen-Truong et al., 2014). Unfortunately, these crucial factors are often overlooked in the literature, particularly, $Cu_2CdSnS_4$ (CCTS)-based solar cells.

CCTS is an exciting quaternary chalcogenide semiconductor that has gained traction as a potential next-generation absorber material for thin film photovoltaics. As a member of the kesterite family, CCTS brings together earth-abundant, non-toxic elements and features a tunable direct band gap ranging from 1.4 to 1.6 eV, along with impressive optical absorption coefficients that exceed $10^4$ $cm^{-1}$. This makes it a strong contender for sustainable and cost-effective solar cell technologies (Xiaolei et al., 2016). When compared to its more widely researched sibling, $Cu_2ZnSnS_4$ (CZTS), the switch from zinc to cadmium in CCTS results in less antisite disorder, better crystallinity, and improved optical performance (Boyang et al., 2024). These characteristics position CCTS as a promising option for absorber layers in thin-film solar cells and optoelectronic devices.

Among the various methods for fabrication, spray pyrolysis stands out as a particularly appealing deposition technique due to its simplicity, scalability, and effectiveness for large-area film growth (Tombak et al., 2019). However, the microstructure, morphology, and optoelectronic properties of CCTS thin films created through spray deposition are quite sensitive to the deposition temperature. This temperature has a direct impact on nucleation and growth kinetics, grain boundary density, and defect states, all of which play a crucial role in controlling carrier dynamics and the overall quality of the absorber layer (Enigochitra et al., 2016; Bakr et al., 2015). Thus, fine-tuning the deposition temperature is essential for producing high-performance CCTS thin films for solar energy conversion.

In addition to structural and optical characteristics, the fundamental electron–phonon interaction ($E_{e\text{-}p}$) in absorber layers is key to understanding carrier transport, recombination, and thermalization. $E_{e\text{-}p}$ refers to the interaction between charge carriers and lattice vibrations, which influences resistivity, carrier lifetime, and thermal conductivity in semiconductors (Giustino, 2017). In thin film absorbers, strong $E_{e\text{-}p}$ can speed up non-radiative recombination, impacting overall efficiency. (Sanjaya et al., 2024, Vettumperumal, et al. 2015). Since the temperature at which deposition occurs plays a crucial role in determining crystalline order and the landscape of defects, it is reasonable to expect that it directly impacts the $E_{e\text{-}p}$ in CCTS thin films.

Moreso, the loss of energy of a fast moving electrons in a material is given in terms of surface energy loss function (SELF) and volume energy loss function (VELF) (Ye-Jin et al., 2023). Notably, SELF describes the probability of fast moving electrons losing energy through the excitation of surface plasmons, which are collective oscillations of free electrons localized at the film surface, while VELF captures the interactions between bulk plasmon and phonon, along with charge screening effects (Caruso et al., 2018; Mkhoyan, 2007).

In this study, we delve into how substrate temperature influences the electron-phonon interactions, as well as the surface and volume energy loss functions of CCTS absorber layers fabricated through spray pyrolysis. By linking deposition conditions to the electron-phonon interaction and energy loss characteristics, this research offers fresh insights into the microscopic interactions between carriers and phonons in CCTS thin films. The results enhance give insight of how growth parameters affect energy dissipation and transport properties, which are vital for optimizing CCTS absorbers in thin-film solar cells.

## MATERIALS AND METHODS

The CCTS thin films were synthesized via the spray pyrolysis method. Precursor solutions were prepared by dissolving high-purity copper (II) acetate ($Cu(CH_3COO)_2 \cdot H_2O$), cadmium acetate dihydrate ($(CH_3COO)_2Cd \cdot 2H_2O$), and tin (IV) chloride ($SnCl_4$) in 2-methoxyethanol, with thiourea ($SC(NH_2)_2$ serving as the sulfur source. A molar ratio of Cu:Cd:Sn:S = 2:1:1:6 was maintained. The solution was stirred thoroughly, after which acetylacetone was added as a stabilizing agent. The mixed solution was then aged for a day to enhance homogeneity and stability. Glass substrates were washed in detergent, acetone, and isopropanol, followed by drying in an oven at 80 °C for 10 minutes. Thin-film deposition was carried out using a Navson Spray Pyrolysis NTPY01 system, maintaining 25 cm as the nozzle to heated substrate distance. The deposition temperature was precisely controlled at 300, 350, and 400 °C, while maintaining constant spray parameters: a flow rate of 0.6 mL/min and a spray interval of 25 minutes to ensure uniform coverage. Following deposition, the films were allowed to cool naturally to room temperature.

The film thickness was measured by the gravimetric method. The structural characteristics of the CCTS thin films were analyzed using an X-ray diffractometer (XRD) (D8 ADVANCE, BRUKER) that utilized Cu-Kα radiation (λ = 1.5406 Å). The XRD measurements were carried out by directing monochromatic Cu-Kα radiation onto the surface of the CCTS thin film and recorded the diffracted X-rays across a selected 2θ range. By analyzing the resulting diffraction patterns were used to identify the crystalline phases in the films by comparing the diffraction peaks to standard reference data from the Joint Committee on Powder Diffraction Standards (JCPDS) database (Cullity and Stock, 2014). The structural parameters of the films were then derived from this diffraction data.

The surface topography of CCTS thin films was analyzed using an Atomic Force Microscope (AFM, Dimension EDGE, BRUKER). In this process, a sharp probe attached to a flexible cantilever moves across the thin film's surface, capturing the interaction forces between the probe tip and the sample. This data is then used to

generate detailed topographic images (Bhushan, 2017). The AFM measurements were conducted over a specific scan area (5µm x 5µm) to assess the surface morphology and roughness characteristics of the deposited CCTS films.

The optical properties of CCTS thin films were investigated using a UV–Visible spectrophotometer (V-750 Series, JASCO). We recorded the absorbance and transmittance spectra of the films across a suitable wavelength range, which typically includes both ultraviolet and visible light. During the measurements, a beam of light was directed at the thin-film sample, and the instrument captured the intensity of the light that passed through compared to the light that hit the sample. From these measurements, the absorbance and transmittance of the films as functions of wavelength were determined (Skoog et al., 2018). This optical data was then used to calculate key parameters like the absorption coefficient, optical band gap, extinction coefficient, refractive index, and dielectric properties of the thin films.

## RESULTS AND DISCUSSION

### Structural Properties of CCTS thin Films

Figure 1 illustrates the XRD pattern of spray-pyrolyzed CCTS thin films at various substrate temperatures, with diffraction angles (2θ) ranging from 10 to 70°. At a deposition temperature of 300 °C, we see diffraction peaks at 28.3°, 46.7°, and 56°. When the substrate temperature is raised to 350 °C, the peaks shift slightly to 28.1°, 47.3°, and 56.3°. For both 300 °C and 350 °C, these diffraction angles align with the (112), (220), and (312) planes, which correspond to the cernyite structure of Cu2CdSnS4, classified under the tetragonal crystal system (Kumar et al., 2017), as per JCPDS card No 29-0537. However, at a deposition temperature of 400 °C, the diffraction peaks appear at 25.9°, 27.9°, 32.3°, 47.9°, and 57.8°, which can be linked to the (101), (112), (200), (220), and (312) planes associated with the stannite structure of CCTS, also within the tetragonal crystal system (Ibraheam et al., 2016). Notably, the most prominent diffraction occurs at the (112) plane, and as the deposition temperature rises, we observe a shift towards lower diffraction angles. This shift may be attributed to lattice expansion, leading to an increase in inter-planar spacing (Amiri et al., 2019), as detailed in Table 1. Additionally, a phase transformation from cernyite to stannite structure is evident with the increase in deposition temperature. The XRD patterns of CCTS films grown at 300, 350, and 400 °C clearly demonstrate this transformation from the cernyite phase to the stannite phase as the substrate temperature increases.

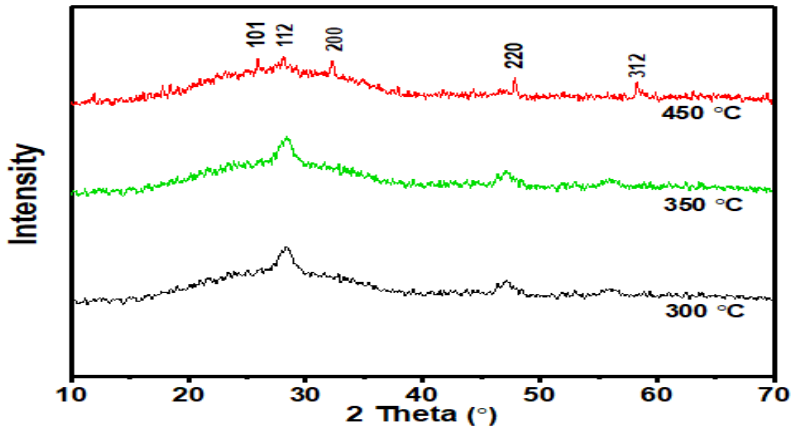


Figure 1: XRD Pattern for $Cu_2CdSnS_4$ Thin Films at Different Substrate Temperatures

The crystallite size (D) , the dislocation density (δ) and the micro-strain (ε) of the CCTS thin films were estimated using Equations 1, 2 and 3 (Ochang et al., 2023) and then presented in Table 1.

$$D = \frac{K\lambda}{\beta \cos\theta} \quad (1)$$

$$\delta = \frac{1}{D^2} \quad (2)$$

$$\varepsilon = \frac{\beta \cos\theta}{4} \quad (3)$$

Where, K is a constant equal to 0.94, $\beta$ is the full width at half maximum (FWHM) in radians of the diffraction peak in radians, θ is the Bragg's angle and λ = 1.5406 Å, wavelength of monochromatic Cu-Kα radiation.

It is observed that, raising the substrate temperature from 300 °C to 400 °C leads to an increase in the average crystallite size from 32.5 nm to 48.3 nm. This change is also accompanied by a drop in dislocation density and microstrain (Table 1). These results point to thermally-driven grain growth and a reduction in defects: as the substrate temperature rises, both surface diffusion and adatom mobility improve, facilitating the merging of smaller grains into larger ones and relaxing micro stresses. (Gunavathy et al., 2019; Bandoh, 2021) Similar

trends have been observed in thin films produced through spray pyrolysis and chemical deposition, where higher deposition and annealing temperatures boost crystallinity and reduce lattice strain (Begum et al., 2012; Mohamed et al., 2016).

The drop in dislocation density at elevated temperatures happens because defects are eliminated and recrystallization takes place during grain growth. However, some residual microstrain might stick around due to thermal stresses and variations in composition. So, while both factors improve with better crystallinity, they don't necessarily decrease at the same pace (Baker, 2000; Ungár and Borbély, 1996).

**Table 1: Structural Properties of Spray Pyrolyzed CCTS Thin Films**

| Substrate Temperature (ºC ) | 2θ(º) | FWHM (radian) | Crystallite size D(nm) | Dislocation density δ x10$^{14}$ (m$^{-2}$) | Microstrain ε x 10$^{-4}$ |
|---|---|---|---|---|---|
| 300 | 28.40 | 0.2573 | 32.51 | 9.5 | 10.88 |
| 350 | 28.00 | 0.1979 | 42.26 | 5.6 | 8.37 |
| 400 | 27.75 | 0.1732 | 48.27 | 4.3 | 7.33 |

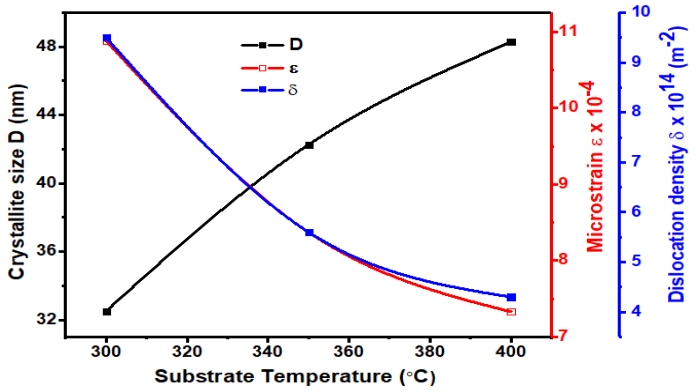


Figure 2: Variation of Crystallite Size, Microstrain and Dislocation Density with Substrate Temperature

**Surface Topography of CCTS Thin Films**

The surface topography of CCTS thin films, as characterized, is illustrated in the 2D and 3D AFM images shown in Figure 3. These AFM images, taken at various substrate temperatures of 300, 350, and 400 °C, depict the topography within a 5μm x 5μm scan area. Figure 4 reports the changes in average surface roughness of the CCTS thin films as the substrate temperature varies. We observed a steady increase in average surface roughness, rising from 64.7 nm at 300 °C to 95.5 nm at 400 °C. This trend can be linked to the increased mobility of adatoms at higher temperatures (Edwin et al., 2020), which encourages grain coarsening, competitive columnar growth (Hall et al., 25), and stress relaxation processes like grooving and hillock formation (Zhou et al., 2023) (see Figure 3b and Figure 3c). These processes ultimately lead to greater peak-to-valley heights on the film surface (Nayak et al., 2024; Reddy and Udayashankar, 2016). Similar patterns of increased roughness with annealing temperature have been noted in oxide and chalcogenide thin films, such as CuO, where grain coalescence and the development of porosity resulted in higher RMS values (Masudy-Panah et al., 2016). Thus, our findings are consistent with existing literature on the roughening regime of temperature-dependent growth, where coarsening and porosity are predominant.

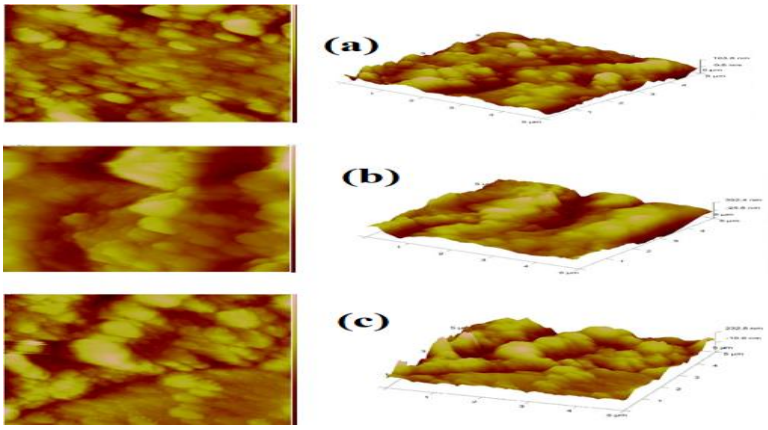


Figure 3: 2D and 3D AFM Images of Spray Pyrolyzed CCTS Thin Films at (a) 300 (˚C), (b) 350 (˚C) and (c) 400 (˚C)

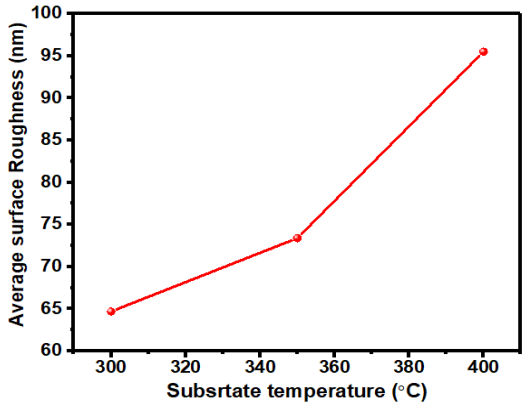


Figure 4: Variation of Average Surface Roughness with Substrate Temperature

**Surface Morphology of $Cu_2CdSnS_4$ Nanomaterial Photoabsorber Layer**

The FE-SEM analysis of CCTS thin films (Figure 5) showed temperature-dependent changes in their surface morphology. At 300 °C, the films had small, loosely packed grains, which resulted in poor surface coverage because the adatoms weren't very mobile. As the temperature was raised to 350 °C, the morphology became more compact and uniform, featuring larger interconnected grains. This change suggests that surface diffusion and grain coalescence were enhanced. At 400 °C, the films displayed densely packed, well-defined grains indicating significant grain growth and better film continuity. However, AFM measurements did reveal a slight increase in surface roughness due to grain coarsening. The larger grains and tighter microstructure at 400 °C are advantageous for minimizing grain-boundary recombination and improving carrier transport, both of which are crucial for photovoltaic performance. These findings align with earlier studies on chalcogenide absorber films, which noted that higher deposition temperatures lead to better grain connectivity and overall morphological quality (Abed et al., 2020). Coupled with the enhanced crystallinity and phase purity seen in the XRD analysis, these results suggest that 400 °C is the ideal deposition temperature for creating high-quality CCTS absorber layers for thin-film solar cells (Ahmed et al., 2019).

In thin-film photovoltaic materials like kesterites, CZTS, CIGS, and other related chalcogenides, films that are smoother and more compact tend to show less electron–phonon scattering, which leads to higher carrier mobility and better photovoltaic performance. On the otherhand, increased roughness often comes with higher defect densities and stronger carrier–phonon interactions, which can ultimately limit the efficiency of the device (Schorr et al., 2020).

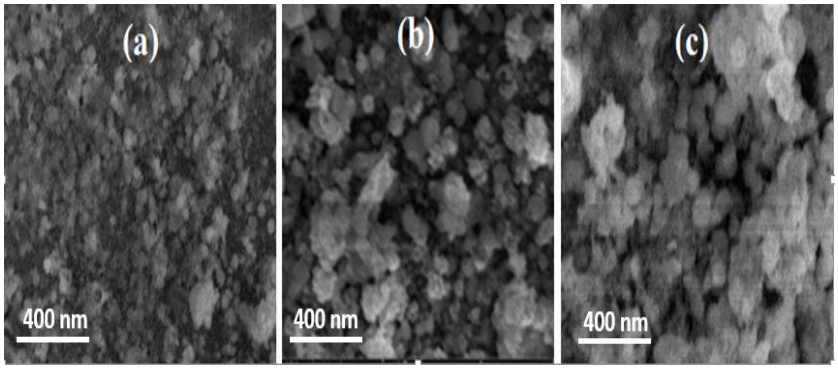


Figure 5: FESEM Images of $Cu_2CdSnS_4$ photoabsorber Layer Deposited at (a) 300 °C, (b) 350 °C and (c) 400 °C

**Elemental Composition of $Cu_2CdSnS_4$ Nanomaterial Photoabsorber Layer**

The elemental composition of CCTS thin films in atomic percent (at. %) as captured by EDS (Fig.6) and reported in Table 2 exhibits a systematic variation with increasing substrate temperature. Specifically, the measured atomic percent of Cu decreases while Cd increases as the temperature rises; Sn shows a minor decrease, and S content also drops gradually. It can be noted that the Cu-poor compositions are the result of shallow acceptors due to the formation of Cu vacancies in the film (Suresh et al., 2020). Moreover, Cu-poor and Sn-poor compositions in the CCTS thin films minimized the formation of $Sn_{Cu}$ anti-site defects, which can limit efficiency in the solar cells (Sun et al., 2023). This trend suggests that elevated temperature processing promotes partial loss of volatile species (notably sulfur) and/ or segregation of Cu-rich species, leading to a relative enrichment of Cd. Such behaviour is consistent with observations in similar Cu-based quaternary sulfide such as CMTS (Chen et al., 2015) CZTS (Surgina et al, 2015), where increased sulfurization or annealing temperatures have been linked to non-stoichiometry and chalcogen loss (Zhang et al., 2017) .This result is in agreement with the XRD results, as there is no detectable $CuS_2$ secondary phase caused by a Cu-rich condition. Also, it is noticed that the compositional ratio of CCTS films is much closer to stoichiometric, even though it is difficult to produce stoichiometric quaternary films by the spray pyrolysis method (Khalate et al., 2017; Kumar et al., 2010; Daranfed et al., 2012)

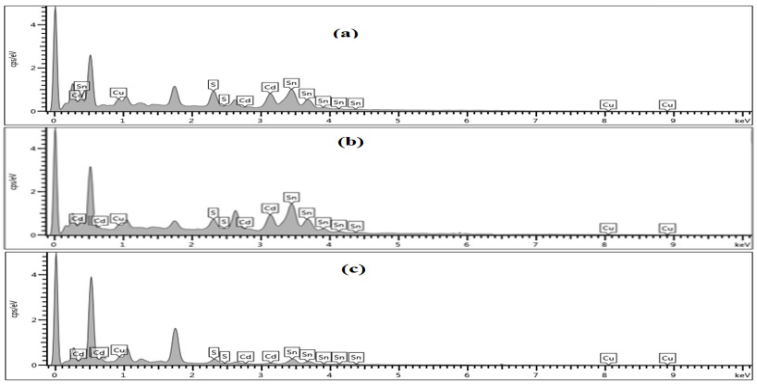


Figure 6: EDS of $Cu_2CdSnS_4$ Photoabsorber Layer Deposited at (a) 300 °C, (b) 350 °C and (c) 400 °C

**Table 2: Elemental Composition (At. %) Analysis of $Cu_2CdSnS_4$ Photoabsorber Layer at Different Deposition Temperature**

| Temp. °C | Cu | Cd | Sn | S | $\frac{Cu}{Cd+Sn}$ | $\frac{Cd}{Cu+Sn}$ | $\frac{Cd}{Sn}$ | $\frac{S}{metal}$ |
|---|---|---|---|---|---|---|---|---|
| 300 | 32.21 | 11.92 | 18.8 | 36.99 | 0.73 | 0.23 | 0.63 | 0.59 |
| 350 | 31.36 | 14.70 | 17.08 | 36.78 | 0.68 | 0.30 | 0.86 | 0.58 |
| 400 | 29.2 | 17.61 | 16.95 | 35.41 | 0.62 | 0.38 | 1.04 | 0.56 |

**Optical Properties of CCTS Thin Films**

***Optical Absorbance***

The absorption spectra of the CCTS thin films (Figure 7a) clearly demonstrate that the substrate temperature has a significant impact on their optical response. Films deposited at 400 °C show a stronger absorbance across the visible spectrum and a more pronounced absorption edge compared to those created at the lower temperature of 300 °C. The observed red-shift of the absorption edge with rising substrate temperature suggests a narrowing of the optical band gap. Similar results have been noted for Cu-based quaternary chalcogenide thin films, where increasing substrate or annealing temperatures slightly decrease the bandgap due to reduced disorder and changes in stoichiometry (Guan, 2021; Tombak et al., 2019). For instance, Tombak et al. (2019) discovered that $Cu_2CdSnS_4$ thin films had absorption coefficients greater than $10^4$ $cm^{-1}$ in the visible range, showing improved absorption and a red-shift in the optical edge after being annealed at higher temperatures. This aligns with our current findings, where we see enhanced absorbance at higher deposition temperatures. Additionally, related research on $Cu_2ZnSnS_4$ (CZTS), which is structurally similar to CCTS, also indicates better optical absorption and sharper absorption edges as the substrate temperature increases (Ahmad et al., 2021). Still, within the moderate substrate temperature range we've examined, the improvements in absorbance and the red-shift of the absorption edge are consistent with the main trends reported in the literature for quaternary chalcogenide absorbers.

**Absorption Coefficient**

To determine the absorption coefficient (α) of the CCTS thin films at varying substrate temperatures, Equation 4 was used.

$$\alpha = \frac{2.303A}{d} \quad (4)$$

Where, $A$ is the absorbance and $d$ represents the film thickness. Figure 7(b) illustrates how α varies with photon energy (hυ) for the CCTS thin films. It can be observed that regardless of the deposition temperatures, the absorption coefficient is ~ $10^5$ $cm^{-1}$, which is comparable to other established photovoltaic absorbers like CIGS (Rawat et al., 2023), CZTS (Henry et al.,2016), and CdTe (Mabvuer et al.,2022, Islam et al., 2013). We observed a consistent rise in α as the deposition temperature increased, likely due to better crystallinity (Ahmed et al., 2020) and grain densification (Bakr et al., 2015). These improvements enhance optical transitions, placing α in the ideal range for efficient photovoltaic applications.

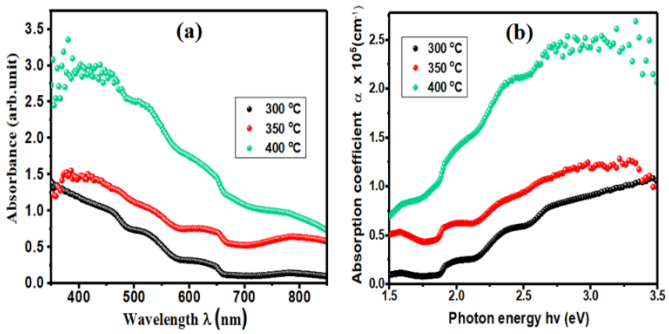


Figure 7: (A) Absorption Spectra (B) Absorption Coefficient of Spray Pyrolyzed CCTS Thin Films at Varying Substrate Temperature

***Optical Bandgap, Refractive Index and Urbach Energy***

The optical band gap values of the CCTS thin films at varying substrate temperature were calculated using the well-established Tauc's relation for direct optical transition given in Equation 5 (Ochang et al., 2023).

$$(\alpha h\upsilon)^2 = B(h\upsilon - E_g) \quad (5)$$

Where, $\alpha$ is the absorption coefficient, $h\upsilon$ is the incident photon energy, $E_{g\ is}$ optical band gap, B is constant. To estimate the optical band gap values, the $(\alpha h\upsilon)^2$ is plotted against $h\upsilon$ as shown in Figure 8. The value of the band gap is obtained by extrapolating the linear portion of the curve on the horizontal axis where $(\alpha h\upsilon)^2 = 0$. The estimated bandgap values are presented in Table 3.

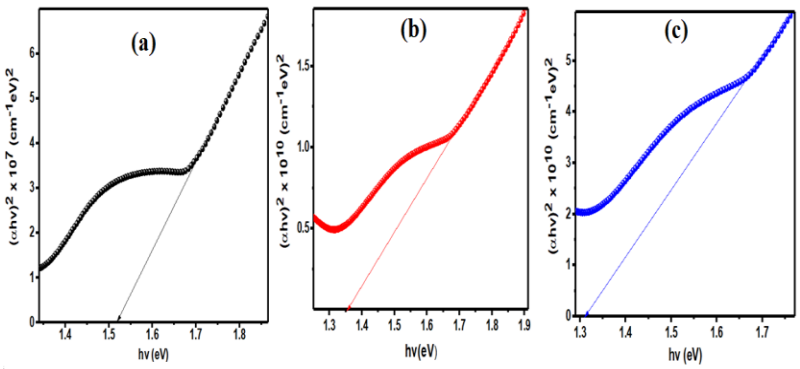


Figure 8: Tauc's Plot for CCTS Thin Films at (A) 300 (˚C), (B) 350 (˚C) and (C) 400 (˚C) Substrate Temperature

The refractive index *n* of the CCTS thin films is calculated using the Herve and Vandamme relation (Equation 6).

$$n = \sqrt{1 + \left[\frac{A}{E_g + B}\right]^2} \qquad (6)$$

Where, $E_g$ is the optical band gap. A = 13.6 eV and B = 3.4 eV. The calculated values of *n* at different substrate temperature are reported in Table 3. The Urbach energy ($E_u$) characterizes the width of the exponential absorption tail extending into the band gap region, which arises from localized states caused by structural disorder, defects, and thermal vibrations (Urbach, 1953). It is determined from the absorption spectra using the Equation 9:

$$\alpha = \alpha_0 exp\frac{h\nu}{E_u} \qquad (9)$$

Where, α is the absorption coefficient, hν the photon energy, and $E_u$ represents the Urbach energy. By plotting ln (α) against photon energy, $E_u$ can be extracted from the inverse of the slope of the linear region of the curve (Figure 9).

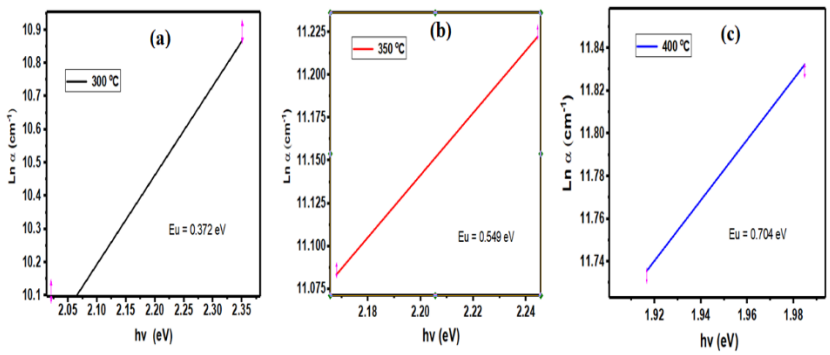


Figure 9: Plots of Ln A Versus Photon Energy CCTS Thin Films at (A) 300 (˚C), (B) 350 (˚C) And (C)400 (˚C) Substrate Temperature

The determined values of the $E_u$ are reported in Table 3. The variation of optical band gap, refractive index and Urbach energy with substrate temperatures is represented in Figure 10. The observed decrease in the optical band gap ($E_g$) with increasing substrate temperature, from 1.52 eV at 300 °C to 1.31 eV at 400 °C, is in good agreement with previous reports on Cu-based quaternary chalcogenides. Guan (2013) reported band gaps in the range of 1.40–1.45 eV for sol–gel deposited CCTS films, while Batir (2024) noted values between 1.35–1.45 eV for well-crystallized CCTS and CZTS thin films. The slight blue-shift observed at lower substrate temperatures in the present study can be attributed to disorder-induced band tailing and smaller grain sizes, which are gradually reduced at higher temperatures, leading to red-shifted band gaps within the intrinsic range of the material. A similar temperature-dependent narrowing of $E_g$ has been reported for CZTS thin films, where annealing improved crystallinity and reduced the density of localized defect states (Ahmad et al., 2021). The refractive index (n) values obtained here (2.94–3.06) also compare well with earlier work. Al-Douri et al. (2018) found a similar range for nanostructured CCTS alloys. The slight increase in n with substrate temperature in this study suggests improved film density and reduced porosity, consistent with reports that higher growth or annealing temperatures enhance grain packing in chalcogenide absorbers. Collectively, the agreement of both $E_g$ and n values with

existing literature underscores the role of substrate temperature in optimizing the optical quality of CCTS films for photovoltaic applications.

It is observed that as the substrate increased from 300 ℃ to 400 ℃, the Urbach energy increased from 0.372 eV to 0.704 eV. The increase in Eu with substrate temperature can be attributed to increase in electron – phonon interaction strength (Makhnovets et al., 2018 and Bonalde et al., 2005) with substrate temperature as seen in Table 3.

**Table 3: Optical Properties and Electron Phonon Interaction of CCTS Thin Films**

| Substrate Temperature (ºC) | Optical Bandgap $E_g$ (eV) | Refractive index n | Urbach energy $E_U$ (eV) | Steepness parameter $\sigma$ | Electron – phonon interaction strength $E_{e-p}$ (eV) |
|---|---|---|---|---|---|
| 300 | 1.52 | 2.94 | 0.372 | 0.133 | 5.03 |
| 350 | 1.36 | 3.03 | 0.549 | 0.098 | 6.83 |
| 400 | 1.31 | 3.06 | 0.704 | 0.082 | 8.10 |

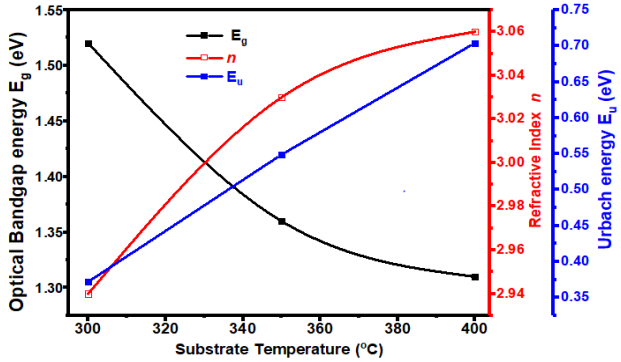


Figure 10: The Variation of Optical Band Gap, Refractive Index and Urbach Energy at Varying Substrate Temperatures

***Electron-Phonon Interaction Strength***

The strength of electron–phonon interaction ($E_{e-p}$) describes the degree to which charge carriers (electrons and holes) interact with lattice vibrations (phonons) within a material. This interaction directly affect resistivity, charge carrier mobility, and optical transitions. In semiconductors and oxide thin films, this coupling governs band-gap renormalization and the formation of Urbach tails that broaden the absorption edge (Urbach, 1953; Jean et al., 2017). The $E_{e-p}$ is related to the Urbach energy $E_u$ according to Equation 10 (Ilkani and Dejam, 2021; Hossain et al., 2016).

$$E_{e-p} = \frac{2}{3\sigma} = \frac{2E_u}{3K_BT} \quad (10)$$

Where, $\sigma$ is the steepness parameter which characterizes the broadening of the optical absorption edge due to the electron–phonon interactions. It is related to the $E_u$ as shown in Equation 11 (Hossain et al., 2016).

$$\sigma = \frac{K_BT}{\mathrm{Eu}} \quad (11)$$

The estimated values of the electron–phonon interaction strength and the steepness parameter of the CCTS thin films are presented in Table 3. While the variation of electron–phonon interaction strength, the steepness parameter and Urbach energy with substrate temperature is presented in Figure 11. The result revealed that the $E_{e-p}$ in CCTS thin films showed a clear relationship with the substrate temperature. A steady increase in $E_{e-p}$, rising from 5.03 at 300 °C to 8.10 at 400 °C was observed. This pattern suggests that higher substrate temperatures boost the coupling between carriers and the lattice vibrations in the films. The rise in $E_{e-p}$ can be attributed to the fact that higher deposition temperatures not only increase the phonon population but also change the microstructural characteristics. In quaternary chalcogenides, elevated substrate temperatures often lead to sulfur volatilization, cation disorder, and the formation of secondary phases. These factors create localized states that interact strongly with phonons (Pishdadian and Ghaleno, 2013). This disorder-driven band tailing is known to enhance phonon-assisted absorption processes, which in turn increases the effective electron–phonon coupling (Sati et al., 2021). The corresponding rise in Urbach energy observed in the same films supports this idea, as Urbach broadening is commonly linked to disorder and electron–phonon interactions (Rambadey et al., 2021).

Similar findings have been noted in other Cu-based quaternary absorbers like $Cu_2ZnSnS_4$ (CZTS). Research indicates that while moderate annealing or deposition temperatures can improve crystallinity and lower defect density, temperatures that exceed the optimal processing range can lead to increased phonon scattering and band tailing (Zaki et al., 2021; Rey, 2018). The consistent increase in $E_{e-p}$ strength from 300 to 400 °C in this study suggests that the films deposited at higher substrate

temperatures went beyond the ideal thermal range, resulting in greater lattice disorder.

From the standpoint of device performance, stronger $E_{e-p}$ is not desirable. It tends to broaden the absorption edge and increase non-radiative recombination losses, which can lead to reduced carrier lifetimes and lower open-circuit voltage in photovoltaic devices (Monserrat et al., 2018; Handa et al., 2018). The the $E_{e-p}$ reported in this study, especially at 400 °C, suggests that while stronger phonon-assisted transitions might enhance light absorption, the charge transport properties are likely to suffer. Therefore, it is essential to optimize spray pyrolysis deposition of CCTS at 400 °C substrate temperature with sulfurization for example to achieve a good balance between crystallinity and minimal electron-phonon coupling strength.

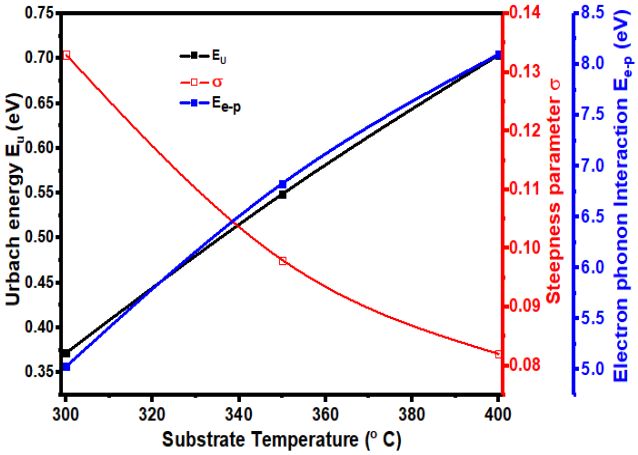


Figure 11: Variation Of Of Electron–Phonon Interaction Strength, Steepness Parameter and Urbach Energy with Substrate Temperature of CCTS Thin Films

***Electron Energy Loss Function in CCTS Thin Films***

The loss of energy of a fast moving electron in a material is given in terms of surface energy loss function (SELF) and volume energy loss function (VELF). SELF describes the probability of fast moving electrons losing energy through the excitation of surface plasmons, which are collective oscillations of free electrons localized at the film surface. Mathematically, SELF is expressed in Equation 12 (Rocca et al., 1995).

$$\text{SELF} = -\text{Im}\left[\frac{1}{\varepsilon+1}\right] = \frac{\varepsilon_2}{(\varepsilon_1+1)^2+\varepsilon_2{}^2} \qquad (12)$$

Where, ε is the complex dielectric function, with $\varepsilon_1$ being the real part and $\varepsilon_2$ the imaginary part. The variation of SELF in CCTS thin films at different temperatures is presented in Figure 12b. It is observed that SELF increases with temperature. The observed increase in SELF in CCTS thin films could be due to improved crystallinity and reduced defects (Mahato et al., 2017; Todorov et al., 2018) as seen in the XRD results in Table 1, Increased film's surface roughness (Lehmann et al., 2014), enhanced carrier concentration and Plasmon resonance (Savariraj et al., 2017) and temperature-driven modulation of dielectric function (Tiwari et al., 2014).

Similar behaviour has been reported in related kesterite thin films such as CZTS and CZTSe. For example, Boutebakh et al. (2025) showed that increasing substrate temperature improved the SELF due to enhanced crystallinity and plasmonic activity. The results in CCTS thin films are therefore consistent with the broader trend in quaternary chalcogenide absorbers, confirming that temperature plays a critical role in modulating plasmonic and dielectric responses.

VELF defines the loss of energy of fast moving electron via characteristic plasma excitation when traveling through bulk of the material. VELF can be determined using Equation 13 (Rocca et al., 1995).

$$\text{VELF} = -\text{Im}\left(\frac{1}{\varepsilon}\right) = \frac{\varepsilon_2}{\varepsilon_1^2+\varepsilon_2^2} \qquad (13)$$

The variation of the volume energy-loss function (VELF) with substrate temperature for CCTS thin films is presented in Figure 12(a). The VELF values increased systematically with substrate temperature, rising from 0.0014 at 300 °C to 0.0016 at 350 °C and reaching 0.0030 at 400 °C. This steady enhancement suggests that higher deposition temperatures promote stronger dielectric resonance within the films. A larger VELF reflects an intensified bulk Plasmon excitation, which is typically associated with improved electronic polarizability and reduced damping of electron oscillations. Such improvements are consistent with the expectation that higher deposition temperatures enhance crystallinity, reduce structural disorder, and increase the mobility of charge carriers (Ahmad et al., 2021).

The modest rise in VELF between 300 °C and 350 °C can be linked to incremental improvements in microstructure, such as slight grain coarsening and defect reduction.

However, the significant increase at 400 °C indicates a more substantial structural transformation. At this temperature, grain growth may become more pronounced, reducing grain boundary scattering, while sulfur vacancies and antisite defects are likely minimized. These microstructural changes improve the dielectric response of the absorber layer, thereby amplifying the VELF. Such observations are in line with annealing studies on $Cu_2ZnSnS_4$ (CZTS) thin films, where higher annealing temperatures enhanced the dielectric strength and sharpened loss-function peaks due to reduced disorder and defect annihilation (Ren, 2017).

Comparing these results with related kesterite-based absorbers confirms the observed trend. In $Cu_2ZnSnS_4$ (CZTS) films, annealing has been reported to enhance the amplitude of the loss function due to improved crystallinity and reduced defects (Ren, 2017). Density functional theory (DFT) studies also reveal that strain relaxation and cation ordering in kesterite-type semiconductors significantly increase the calculated energy-loss function values (Yang et al., 2022).The observed increase at 400 °C in the present work therefore strongly suggests that the film structure approaches a more ordered and stoichiometric state at this temperature. Nevertheless, care must be taken since excessive heating beyond this range can cause sulfur loss or secondary phase formation, leading to degraded electronic properties (Ren, 2017). On the other hand, spray pyrolysis deposition of CCTS above this temperature can be done in sulphur atmosphere.

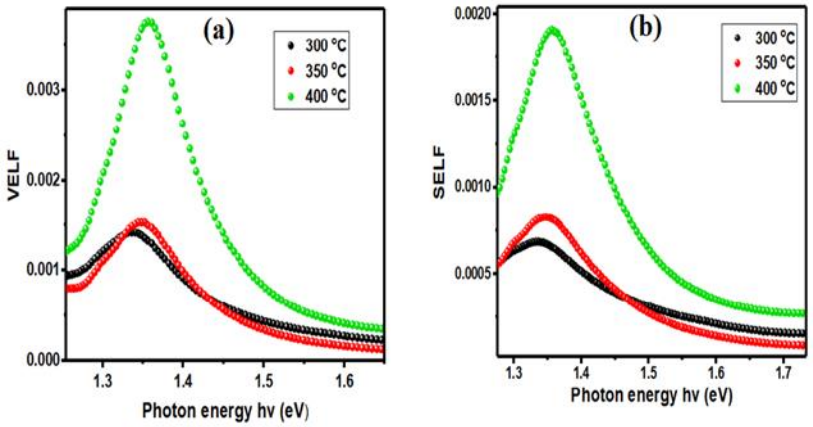


Figure 12: (A) Volume Energy Loss Function and (B) Surface Energy Loss Function of Spray Pyrolyzed CCTS Thin Films at Different Substrate Temperature

## CONCLUSION

The current study effectively explored how substrate temperature affects the electron–phonon interaction and the electron energy loss function (EELF) of spray-pyrolyzed $Cu_2CdSnS_4$ (CCTS) thin films that deposited at temperatures ranging from 300 to 400 °C. The findings showed that icreasing the substrate temperature significantly enhanced the structural quality of the films. This was evident through improved crystallinity, larger crystallite sizes, reduced microstrain, and lower dislocation density. These structural enhancements also led to better optical and dielectric properties, such as high absorption coefficients (~$10^5$ $cm^{-1}$), a smaller optical band gap, and increases in the refractive index, dielectric constant, electronic polarizability, and optical susceptibility. The investigation into the electron–phonon interaction revealed that the changes in electronic structure and dielectric response are heavily influenced by temperature-driven microstructural alterations, which affect carrier–lattice coupling and energy dissipation processes. One of the key contributions of this research is the thorough connection made between structural changes, electron-phonon interactions, electron energy loss behaviour, and the optoelectronic performance of CCTS thin films. This offers valuable insights into the fundamental mechanisms that drive carrier dynamics in this absorber material. However, the study does have its limitations, particularly due to the lack of direct electrical transport and spectroscopic investigations, like Hall-effect and photoluminescence measurements, which could further validate the parameters derived optically. Overall, the film that was deposited at 400 °C showed the best combination of structural, dielectric, and optoelectronic properties, underscoring its potential as an effective absorber layer in thin-film photovoltaic and optoelectronic devices.

## REFERENCES

Abed, M. A., Bakr, N. A., & Al-Zanganawee, J. M. (2020**).** Structural, optical and electrical properties of $Cu_2NiSnS_4$ thin films deposited by chemical spray pyrolysis method. *Chalcogenide Letters, 17*(4), 179–186. https://doi.org/10.15251/CL.2020.174.179

Ahmad, A. A., Migdadi, A. B., Alsaad, A. M., Qattan, I. A., Al-Bataineh, Q. M., & Telfah, A. (2021). Computational and experimental characterizations of annealed $Cu_2ZnSnS_4$ thin films. *Heliyon, 8*(1), e08683. https://doi.org/10.1016/j.heliyon.2021.e08683

Ahmed, M. A., Bakr, N. A., & Kamil, A. A. (2019). Synthesis and characterization of chemically sprayed $Cu_2CoSnS_4$ thin films. *Chalcogenide Letters, 16*(5), 231–239.

Ahmed, H. J., Kamil, A. A., Habeeb, A. A., & Bakr, N. A. (2020). The influence of deposition temperature on the properties of chemically sprayed nanostructured $Cu_2CdSnS_4$ thin films. *International Research Journal of Science and Technology, 1*(2), 149–155. https://doi.org/10.46378/irjst.2020.010211

Al-Douri, Y., Odeh, A. A., Johan, M. R., Chowdhury, Z. Z., Rafique, R. F., Reshak, A. H., & Voon, C. H. (2018). Synthesis and characterization of $Cu_2CdSnS_4$ quaternary alloy nanostructures. *International Journal of Electrochemical Science, 13*, 6693–6707. https://doi.org/10.20964/2018.07.45

Alkauskas, A., Yan, Q., & Van de Walle, C. G. (2014**).** First-principles theory of nonradiative carrier capture via multiphonon emission. *Physical Review B, 90*(7), 075202. https://doi.org/10.1103/PhysRevB.90.075202

Baker, I. (2000). Recovery, recrystallization and grain growth in ordered alloys. *Intermetallics, 8*(9–11), 1183–1196. https://doi.org/10.1016/S0966-9795(00)00031-5

Bakr, N. A., Khodair, Z. T., & Abdul Hassan, S. M. (2015). Effect of substrate temperature on structural and optical properties of $Cu_2ZnSnS_4$ (CZTS) films prepared by chemical spray pyrolysis method. *Research Journal of Chemical Sciences, 5*(10), 51–61.

Bandoh, C. K., Nkrumah, I., Ampong, F. K., Nkum, R. K., & Boakye, F. (2021). Effect of annealing on the structure and optical properties of lead selenide and cadmium selenide thin film prepared by chemical bath deposition. *Chalcogenide Letters, 18*(2), 81–89.

Begum, A., Hussain, A., & Rahman, A. (2012). Effect of deposition temperature on the structural and optical properties of chemically prepared nanocrystalline lead selenide thin films. *Beilstein Journal of Nanotechnology, 3*, 438–443. https://doi.org/10.3762/bjnano.3.50

Bhushan, B. (2017). *Scanning probe microscopy in nanoscience and nanotechnology* (3rd ed.). Springer.

Bonalde, I., Medina, E., & Wasim, S. M. (2005). Temperature dependence of the Urbach energy in ordered defect compounds $Cu\text{-}III_3\text{-}VI_5$ and $Cu\text{-}III_5\text{-}VI_8$. *Journal of Physics and Chemistry of Solids, 66*(10), 1865–1867. https://doi.org/10.1016/j.jpcs.2005.10.002

Boriskina, S. V., Cooper, T. A., Zeng, L., Ni, G., Tong, J. K., Tsurimaki, Y., Huang, Y., Meroueh, L., Mahan, G., & Chen, G. (2017). Losses in plasmonics: From mitigating energy dissipation to embracing loss-enabled functionalities. *Advances in Optics and Photonics, 9*(4), 775–827. https://doi.org/10.1364/AOP.9.000775

Boutebakh, F. Z., Attaf, N., & Aida, M. S. (2025). Effect of growth temperature on the physical properties of kesterite $Cu_2ZnSnS_4$ (CZTS) thin films. *Discover Materials, 5*, Article 4. https://doi.org/10.1007/s43939-025-00179-w

Boyang, H., Li, Y., Wang, R., Zhu, W., He, Z., Sun, H., Meng, X., Huang, S., Song, Y., & Zhang, J. (2024). Viable strategy for suppressing antisite defects and band tailing states in solution-processed kesterite solar cells via IIIA incorporation: Case of aluminum. *ACS Applied Energy Materials, 7*(16), 7074–7084. https://doi.org/10.1021/acsaem.4c01475

Brahma, S., Lo, C.-Y., Chen, S.-C., Chu, H.-C., Hsu, C. H., & Huang, J.-L. (2024). Defect-induced crystal lattice disorder and its effect on the electron–phonon coupling in Fe-doped ZnO thin films. *Journal of Physics and Chemistry of Solids, 190*, 111999. https://doi.org/10.1016/j.jpcs.2024.111999

Caruso, F., Novko, D., & Draxl, C. (2018). Phonon-assisted damping of plasmons in three- and two-dimensional metals. *Physical Review B, 97*(20), 205118. https://doi.org/10.1103/PhysRevB.97.205118

Chen, L., Deng, H., Tao, J., Zhou, W., Sun, L., Yue, F., Yang, P., & Chu, J. (2015). Influence of annealing temperature on structural and optical properties of $Cu_2MnSnS_4$ thin films fabricated by sol-gel technique. *Journal of Alloys and Compounds*. https://doi.org/10.1016/j.jallcom.2015.03.225

Cullity, B. D., & Stock, S. R. (2014**).** *Elements of X-ray diffraction* (3rd ed.). Pearson Education Limited.

Daranfed, W., Aida, M. S., Attaf, N., Bougdira, J., & Rinnert, H. (2012). $Cu_2ZnSnS_4$ thin films deposition by ultrasonic spray pyrolysis. *Journal of Alloys and Compounds, 542*, 22–

Dizaj, M. H**.** (2025). Recombination mechanisms in perovskite materials: A theoretical and experimental

perspective. *Journal of Science and Engineering Elites*. http://www.elitesjournal.ir

Enigochitra, A.S., P. Perumal, C. Sanjeeviraja, D. Deivamani, M. Boomashri. (2016).Influence of substrate temperature on structural and optical properties of ZnO thin films prepared by cost-effective chemical spray pyrolysis technique, Superlattices and Microstructures. 90:313-320, https://doi.org/10.1016/j.spmi.2015.10.026.

Giustino, F. (2017). Electron–phonon interactions from first principles. *Reviews of Modern Physics, 89*(1), 015003. https://doi.org/10.1103/RevModPhys.89.015003

Gunavathy, K.V., K. Tamilarasan, C. Rangasami, A.M.S. Arulanantham (2019). A review on growth optimization of spray pyrolyzed $Cu_2ZnSnS_4$ chalcogenide absorber thin film, *International Journal of Energy Research* .https://doi.org/10.1002/er.4693.

Handa, T., Aharen, T., Wakamiya, A., & Kanemitsu, Y. (2018). Radiative recombination and electron–phonon coupling in lead-free $CH_3NH_3SnI_3$ perovskite thin films. *Physical Review Materials, 2*(7), 075402. https://doi.org/10.1103/PhysRevMaterials.2.075402

Hao Guan, Jingchuan Zhao , Xu Wang , Fangli Yu (2013) Cu2CdSnS4 Thin Film Prepared by a Simple Solution Method. Chalcogenide Letters Vol. 10, No. 10, October 2013, P. 367 – 372.

Henry, J, Mohanraj, K.,. Sivakumar, G .(2016).Electrical and optical properties of CZTS thin films prepared by SILAR method,_ Journal of Asian Ceramic Societies, 4(1): 81-84. https://doi.org/10.1016/j.jascer.2015.12.003

Hossain, M. D. S., Kabir, H., Rahman, M. M., Hasan, K., Bashar, M. S., Rahman, M., Gafur, M. A., Islam, S. H., Amri, A., Jiang, Z. T., Altarawneh, M., & Dlugogorskii, B. Z. (2016). Understanding the shrinkage of optical absorption edges of nanostructured Cd–Zn sulphide films for photothermal applications. *Applied Surface Science, 392*, 1038–1046. https://doi.org/10.1016/j.apsusc.2016.09.095

Ibraheam, A. S., Al-Douri, Y., Al-Hazeem, N. Z., Hashim, U., Prakash, D., & Verma, K. D. (2016). Effect of cadmium concentration on structural, optical, and electrical properties of $Cu_2Zn_{1-x}Cd_xSnS_4$ quinternary alloy nanofibres synthesized by electrospinning technique. *Journal of Nanomaterials, 2016*, Article 7314714. https://doi.org/10.1155/2016/7314714

Islam, M. (2013). High quality 1 μm thick CdTe absorber layers grown by magnetron sputtering for solar cell application. *Current Applied Physics, 13*(1), 115–121. https://doi.org/10.1016/j.cap.2013.02.015

Joel, J., Mahony, T. S., Bozyigit, D., Sponseller, M., Holovsky, J., Bawendi, M. G., & Bulovic, V. (2017). Radiative efficiency limit with band tailing exceeds 30% for quantum dot solar cells. *ACS Energy Letters, 2*(11), 2616–2624. https://doi.org/10.1021/acsenergylett.7b00923

Khalate, S. A., Kate, R. S., Kim, J. H., Pawar, S. M., & Deokate, R. J. (2017). Effect of deposition temperature on the properties of $Cu_2ZnSnS_4$ (CZTS) thin films. *Superlattices and Microstructures, 103*, 335–342. https://doi.org/10.1016/j.spmi.2017.02.003

Kumar, Y. B. K., Bhaskar, P. U., Babu, G. S., & Raja, V. S. (2010). Effect of copper salt and thiourea concentrations on the formation of $Cu_2ZnSnS_4$ thin films by spray pyrolysis. *physica status solidi (a), 207*(1), 149–156. https://doi.org/10.1002/pssa.200925194

Kumar, M. S., Mohanta, K., & Batabyal, S. K. (2017). Solution processed $Cu_2CdSnS_4$ as a low-cost inorganic hole transport material for polymer solar cells. *Solar Energy Materials and Solar Cells, 161*, 157–161. https://doi.org/10.1016/j.solmat.2016.11.028

Lehmann, D., Seidel, F., & Zahn, D. R. (2014). Thin films with high surface roughness: Thickness and dielectric function analysis using spectroscopic ellipsometry. *SpringerPlus, 3*, 82. https://doi.org/10.1186/2193-1801-3-82

Liu, X., Feng, Y., Cui, H., Liu, F., Hao, X., Conibeer, G., Mitzi, D. B., & Green, M. A. (2016). The current status and future prospects of kesterite solar cells: A brief review. *Progress in Photovoltaics: Research and Applications, 24*(6), 879–898. https://doi.org/10.1002/pip.2741

Mabvuer, F. T., Nya, F. T., & Kenfack, G. M. D. (2022). Improving the absorption spectrum and performance of CIGS solar cells by optimizing the stepped band gap profile of the multilayer absorber. *Solar Energy, 240*, 193–200. https://doi.org/10.1016/j.solener.2022.05.037

Mahato, S., Patel, M., & Bhattacharya, P. (2017). Influence of deposition temperature on structural, optical and dielectric properties of CZTS thin films. *Materials Research Bulletin, 95*, 410–418. https://doi.org/10.1016/j.materresbull.2017.08.028

Makhnovets, G. V., Myronchuk, G. L., Piskach, L. V., Vidrynskyi, B. V., & Kevshyn, A. H. (2018). Study of optical absorption in $TlGaSe_2:Zn^{2+}$ single crystals.

*Ukrainian Journal of Physical Optics, 19*(1), 49–59. https://doi.org/10.3116/16091833/19/1/49/2018

Ilkhani, M., & Dejam, L. (2021). Structural and optical properties of ZnO and Ni:ZnO thin films: The trace of post-annealing. *Journal of Materials Science: Materials in Electronics, 32*, 3460–3474. https://doi.org/10.1007/s10854-020-05092-x

Mkhoyan, K. A., Babinec, T., Maccagnano, S. E., Kirkland, E. J., & Silcox, J. (2007). Separation of bulk and surface losses in low-loss EELS. *Ultramicroscopy, 107*(4–5), 345–355. https://doi.org/10.1016/j.ultramic.2006.09.003

Mohamed, J. R., Sanjeeviraja, C., & Amalraj, L. (2016). Influence of substrate temperature on physical properties of (111) oriented $CdIn_2S_4$ thin films by nebulized spray pyrolysis technique. *Journal of Asian Ceramic Societies, 4*(2), 191–200. https://doi.org/10.1016/j.jascer.2016.03.002

Monserrat, B., Park, J.-S., Kim, S., & Walsh, A. (2018). Role of electron–phonon coupling and thermal expansion on band gaps, carrier mobility, and interfacial offsets in kesterite thin-film solar cells. *Applied Physics Letters, 112*(19), 193903. https://doi.org/10.1063/1.5028186

Nguyen-Truong, H. T. (2014). Energy-loss function including damping and prediction of plasmon lifetime. *Journal of Electron Spectroscopy and Related Phenomena, 196*, 23–29. https://doi.org/10.1016/j.elspec.2014.03.010

Pishdadian, S., & Ghaleno, A. M. S. (2013). Influences of annealing temperature on the optical and structural properties of manganese oxide thin film by Zn doping from sol-gel technique. *Acta Physica Polonica A, 123*(4), 741–745. https://doi.org/10.12693/APhysPolA.123.741

Rambadey, O. V., Kumar, A., Sati, A., & Sagdeo, P. R. (2021). Exploring the interrelation between Urbach energy and dielectric constant in Hf-substituted $BaTiO_3$. *ACS Omega, 6*(47), 32231–32238. https://doi.org/10.1021/acsomega.1c05057

Ren, Y. I. (2017). *Annealing of $Cu_2ZnSn(S,Se)_4$ thin films: A study of secondary compounds and their effects on solar cells* (Digital Comprehensive Summaries of Uppsala Dissertations from the Faculty of Science and Technology No. 1476). Uppsala University. ISSN 1651-6214. urn:nbn:se:uu:diva-314975

Rey, G., Larramona, G., Bourdais, S., Choné, C., Delatouche, B., Jacob, A., Dennler, G., & Siebentritt, S. (2018). On the origin of band-tails in kesterite. *Solar Energy Materials and Solar Cells, 179*, 142–151. https://doi.org/10.1016/j.solmat.2017.11.005

Rocca, M., Lindau, I., & Onellion, M. (1995). Energy-loss functions and surface plasmons in semiconductors. *Surface Science Reports, 22*(1), 1–54. https://doi.org/10.1016/0167-5729(94)00006-7

Rondiya, S. R., Jadhav, Y. A., Živković, A., Jathar, S. B., Rahane, G. K., Cross, R. W., Rokade, A. V., Devan, R. S., Kolekar, S., Hoye, R. L. Z., de Leeuw, N. H., Jadkar, S. R., & Dzade, N. Y. (2022). Solution-processed Cd-substituted CZTS nanocrystals for sensitized liquid junction solar cells. *Journal of Alloys and Compounds, 890*, 161575. https://doi.org/10.1016/j.jallcom.2021.161575

Aanchal, S., Kumar, A., Mishra, V., Warshi, K., Pokhriyal, P., Sagdeo, A., & Sagdeo, P. R. (2021). Temperature-dependent dielectric loss in $BaTiO_3$: Competition between tunnelling probability and electron–phonon interaction. *Materials Chemistry and Physics, 257*, 123792. https://doi.org/10.1016/j.matchemphys.2020.123792

Rawat, S., Gupta, R., & Gohri, S. (2023). Performance assessment of CIGS solar cell with different CIGS grading profile. *Materials Today: Proceedings*. https://doi.org/10.1016/j.matpr.2023.03.356

Wang, S., Peng, Y., Li, L., Zhou, Z., Liu, Z., Zhou, S., & Yao, M. (2022). Impact of loss mechanisms on performances of perovskite solar cells. *Physica B: Condensed Matter, 647*, 414363. https://doi.org/10.1016/j.physb.2022.414363

Skoog, D.A., Holler, F.J. and Crouch, S.R. (2017) Principal of Instrumental Analysis. 7th Edition, Sunder College Publisher, New York.

Schorr, S., Gurieva, G., Guc, M., Dimitrievska, M., Pérez-Rodríguez, A., Izquierdo-Roca, V., Schnohr, C., Merino, J. M., Kim, J., & Jo, W. (2020). Point defects, compositional fluctuations, and secondary phases in non-stoichiometric kesterites. *Journal of Physics: Energy, 2*(1), Article 012002. https://doi.org/10.1088/2515-7655/ab4a25

Sun, K., Huang, J., Li, J., Yan, C., & Hao, X. (2023). Recent progress in defect engineering for kesterite solar cells. *Science China Physics, Mechanics & Astronomy, 66*, Article 217302. https://doi.org/10.1007/s11433-022-1939-6

Suresh, K. M., Sreejith, P., Athimotlu, R. R., Mohamed, S., & Sudip, K. B. (2020). Barium (Ba) substitution in

kesterite $Cu_2ZnSnS_4$: $Cu_2Zn_{1-x}Ba_xSnS_4$ (CZBTS) quinary alloy thin films for efficient solar energy harvesting. *Crystal Growth & Design*. *(Please verify volume, issue, page numbers, and DOI, as the DOI provided appears inconsistent with the journal title.)*

Surgina, G. D., Nevolin, V. N., Sipaylo, I. P., Teterin, P. E., Medvedeva, S. S., Lebedinsky, Y. Y., & Zenkevich, A. V. (2015). Effect of annealing on structural and optical properties of $Cu_2ZnSnS_4$ thin films grown by pulsed laser deposition. *Thin Solid Films*. https://doi.org/10.1016/j.tsf.2015.10.014

Savariraj, D., Kim, H.-J., Karuppanan, S., & Prabakar, K. (2017). Phase transformation and evolution of localized surface plasmon resonance in $Cu_2$–xS thin films deposited at 60 °C. *The Journal of Physical Chemistry C, 121*(45), 25440–25446. https://doi.org/10.1021/acs.jpcc.7b07332

Tiwari, D., Chaudhuri, T. K., Shripathi, T., Deshpande, U., & Sathe, V. G. (2014). Structural and optical properties of layer-by-layer solution deposited $Cu_2SnS_3$ films. *Journal of Materials Science: Materials in Electronics, 25*, 3687–3694. https://doi.org/10.1007/s10854-014-2076-y

Tombak A, Kilicoglu T, Ocak YS, (2019).Solar cells fabricated by spray pyrolysis deposited $Cu_2CdSnS_4$ thin films, Renewable Energy, doi: https://doi.org/10.1016/j.renene.2019.07.057

Ungár, T., and Borbély, A. (1996). The effect of dislocation contrast on X-ray line broadening: A new approach to line profile analysis. *Applied Physics Letters, 69*(21), 3173–3175. https://doi.org/10.1063/1.117951

Vettumperumal, R. S. Kalyanaraman, B. Santoshkumar, R. Thangavel, (2015). Estimation of Electron-Phonon coupling and Urbach Energy in Group I elements doped ZnO Nanoparticles and Thin Films by Sol-Gel Method, Materials Research Bulletin http://dx.doi.org/10.1016/j.materresbull.2016.01.015

Yang, X., Qin, X., Yan, W., Zhang, C., Zhang, D., & Guo, B. (2022). Electronic Structure and Optical Properties of $Cu_2ZnSnS_4$ under Stress Effect. *Crystals*, *12*(10), 1454. https://doi.org/10.3390/cryst12101454

Ye-Jin K, Levi D. Palmer, Wonseok L, Nicholas J. Heller, Scott K. C. (2023). Using electron energy-loss spectroscopy to measure nanoscale electronic and vibrational dynamics in a TEM. Journal of Chemical Physics. https://doi.org/10.1063/5.0147356

Zaki, M.-Y., Sava, F., Buruiana, A.-T., Simandan, I.-D., Becherescu, N., Galca, A.-C., Mihai, C., & Velea, A. (2021). *Synthesis and Characterization of $Cu_2ZnSnS_4$ Thin Films Obtained by Combined Magnetron Sputtering and Pulsed Laser Deposition*. *Nanomaterials, 11*(9), 2403. https://doi.org/10.3390/nano11092403

Zhang, Q., Deng, H., Chen, L., Tao, J., Yu, J., Yang, P., & Chu, J. (2017). Effects of sulfurization temperature on the structural and optical properties of $Cu_2CdSnS_4$ thin films prepared by direct liquid method. *Materials Letters, 193*, 206–209. https://doi.org/10.1016/j.matlet.2017.02.002

Zhenzhu Z, Mulin S Fang X, Xuefei W, Zachary F, Zongming H, Junyao G, Honghe D, Pengju T, Chengjian Y, Yuqian Y, Nikita A. Emelianov, Lyubov A. Frolova, Zhengguo Xiao, Pavel A. Troshin, Thomas P. Russell, Junfa Zhu, Yu Li and Qin Hu (2024). Enhanced charge carrier extraction and transport with interface modification for efficient tin-based perovskite solar cells. *J. Mater. Chem. A*, 2025,13, 409-417. https://doi.org/10.1039/D4TA06046F

Zhu J., Tang, M, B. He, W. Zhang, X. Li, Z. Gong, H. Chen, Y. Duan and Q. Tang(2020). Improved charge extraction through interface engineering for 10.12% efficiency and stable $CsPbBr_3$ perovskite solar cells. J. Mater. Chem. A, https://doi.org/10.1039/D0TA08675D